Biochimica et Biophysica Acta 1837 (2014) 277–286

Contents lists available at ScienceDirect

Biochimica et Biophysica Acta

journal homepage: www.elsevier.com/locate/bbabio

Reductive activation in periplasmic nitrate reductase involves chemical modifications of the Mo-cofactor beyond the first coordination sphere of the metal ion

Julien G.J. Jacques [a], Vincent Fourmond [a], Pascal Arnoux [b], Monique Sabaty [b], Emilien Etienne [a], Sandrine Grosse [b], Frédéric Biaso [a], Patrick Bertrand [a], David Pignol [b], Christophe Léger [a], Bruno Guigliarelli [a], Bénédicte Burlat [a,*]

[a] Aix-Marseille Université, CNRS, BIP UMR 7281, 31 chemin J. Aiguier, F-13402 Marseille cedex 20, France
[b] Aix-Marseille Université, CNRS, CEA, DSV/IBEB/LBC UMR 7265, F-13108 Saint Paul Lez Durance, France

ARTICLE INFO

Article history:
Received 18 June 2013
Received in revised form 24 October 2013
Accepted 30 October 2013
Available online 7 November 2013

Keywords:
Molybdenum
Nitrate reductase
Pyranopterin
Electron transfer
Protein film voltammetry
EPR spectroscopy

ABSTRACT

In *Rhodobacter sphaeroides* periplasmic nitrate reductase NapAB, the major Mo(V) form (the "high *g*" species) in air-purified samples is inactive and requires reduction to irreversibly convert into a catalytically competent form (Fourmond et al., J. Phys. Chem., 2008). In the present work, we study the kinetics of the activation process by combining EPR spectroscopy and direct electrochemistry. Upon reduction, the Mo (V) "high *g*" resting EPR signal slowly decays while the other redox centers of the protein are rapidly reduced, which we interpret as a slow and gated (or coupled) intramolecular electron transfer between the [4Fe–4S] center and the Mo cofactor in the inactive enzyme. Besides, we detect spin–spin interactions between the Mo(V) ion and the $[4Fe–4S]^{1+}$ cluster which are modified upon activation of the enzyme, while the EPR signatures associated to the Mo cofactor remain almost unchanged. This shows that the activation process, which modifies the exchange coupling pathway between the Mo and the $[4Fe–4S]^{1+}$ centers, occurs further away than in the first coordination sphere of the Mo ion. Relying on structural data and studies on Mo-pyranopterin and models, we propose a molecular mechanism of activation which involves the pyranopterin moiety of the molybdenum cofactor that is proximal to the [4Fe–4S] cluster. The mechanism implies both the cyclization of the pyran ring and the reduction of the oxidized pterin to give the competent tricyclic tetrahydropyranopterin form.

1. Introduction

Periplasmic nitrate reductases (Nap) are soluble molybdenum-containing enzymes found in Prokaryotes. These dissimilatory enzymes catalyze the two-electron and two-proton reduction of nitrate into nitrite [1]. So far, periplasmic nitrate reductases have been purified from *Paracoccus pantotrophus* (formerly *Paracoccus denitrificans*) [2], *Desulfovibrio desulfuricans* [3], *Rhodobacter sphaeroides* [4], *Cupriavidus necator* (formerly *Ralstonia eutropha*) [5], *Escherichia coli* [6] and *Shewanella gelidimarina* [7]. Besides, soluble bacterial assimilatory nitrate reductases (Nas), closely related to Nap enzymes, have been isolated and characterized [8–10]. With the exception of the monomeric NapA from *D. desulfuricans* which directly receives electrons from the membrane-bound tetraheme NapC, Nap enzymes form heterodimeric complexes. The NapA catalytic subunit (75–90 kDa) houses both the molybdenum cofactor where substrate binds and a [4Fe–4S] center; the NapB subunit (15 kDa) uses two *c*-type hemes to mediate electrons from NapC to NapA. The strength of the interaction between NapA and NapB is organism-dependent: nitrate reductases from *E. coli* or *S. gelidimarina* purify as a monomer (NapA), while nitrate reductases from *P. pantotrophus* and *R. sphaeroides* are isolated as tight NapAB heterodimers [6,7,11].

Several crystallographic structures of NapA (*D. desulfuricans* [12,13] and *E. coli* [6]) and NapAB (*R. sphaeroides* [11] and *C. necator* [14]) unveil the structural characteristics of the Mo-bis(pyranopterin-guanosine-dinucleotide or PGD) cofactor (Mo-cofactor) of the molybdo-enzymes from the DMSO reductase family. Within this large cofactor of about 1.6 kDa the molybdenum ion is coordinated by two dithiolene ligands from the pyranopterins (often named molybdopterins) and one thiolate ligand from a cysteine which is the only covalent anchor of the cofactor to the protein. An inorganic ligand completes the coordination sphere of the Mo ion; it was formerly modeled as an oxygenated species (hydroxo or water ligand [6,12]) and has been more recently reinterpreted as a sulfur atom forming a partial disulfide bond with the sulfur of the cysteine ligand [13,14].

These recent structural data called for reconsidering the catalytic mechanism of Nap, particularly the coordination mode of nitrate to

* Corresponding author at: Unité de Bioénergétique et Ingénierie des Protéines UMR7281, CNRS/AMU, FR3479, F-13402 Marseille Cedex 20, France. Tel.: +33 491 164 559; fax: +33 491 164 097.
E-mail address: burlat@imm.cnrs.fr (B. Burlat).

0005-2728/$ – see front matter © 2013 Elsevier B.V. All rights reserved.
http://dx.doi.org/10.1016/j.bbabio.2013.10.013

the Mo-cofactor and the oxo transfer reaction. New proposals came from theoretical studies (recently reviewed in refs [15,16]). Both inner- and outer-sphere mechanisms have been investigated. In the former, nitrate is an extra ligand of the Mo ion, which either extends its coordination number to 7, or undergoes a "sulfur-shift" mechanism that allows the binding of nitrate on its sixth position [17–19]. Outer-coordination sphere mechanisms investigate the possibility of nitrate binding to the inorganic sulfido ligand of the Mo during turnover [17,18]. While initial mechanisms considered that the oxidation degree of the Mo ion ranges from + IV to + VI, the question of the Mo valence during catalysis, and notably the role of the Mo^V state, remain debated in the last mechanisms. The Mo^V state ($4d^1$) being paramagnetic with a spin $S = 1/2$, Mo(V) intermediates of the Mo-cofactor related to redox regeneration during catalysis, and/or substrate-bound Mo(V) species, can be detected by EPR spectroscopy.

All EPR studies have shown the plasticity of the Mo coordination sphere in soluble nitrate reductases. Many Mo(V) species have been detected and classified in three groups: "high *g*", "very high *g*" and "low *g*", the last two being minor species. The "low *g*" form, occasionally observed in reduced states of Nap, has been assigned to a degradation product with only one pyranopterin-unit binding the Mo [20]. The catalytic relevance of the "very high *g*" species that is also detected in the resting state of Nas enzymes is still unclear. Several Mo(V) "high *g*" species could be identified depending on purification conditions, on sample treatment, and on the organism of origin. The so-called "high *g*" state was observed in *as prepared* samples of NapAB from *P. pantotrophus* [2], *R. sphaeroides* [11] and NapA from *S. gelidimarina* [7], in reduced samples of *Syneccochus elongatus* NarB [9] and also in turnover conditions in *P. pantotrophus* NapAB [21]. Another form, named "high *g* nitrate", was observed after enzyme reduction in the presence of nitrate in *P. pantotrophus* NapAB [20], *D. desulfuricans* NapA [3] and in *Azotobacter vinelandii* Nas [8], but also upon reduction without nitrate in *E. coli* NapA [6]. A third species, giving the "high *g* turnover" signal, was obtained in *D. desulfuricans* NapA in the presence of nitrate and reduced methyl viologen [22]. Other "high *g*" species have been observed when Nap is treated with inhibitors, azide and thiocyanide [20,22,23]. In addition, other minor Mo(V) signals with different *g*-values have been reported in studies of *D. desulfuricans* NapA [22]. All these "high *g*" signals share common features suggesting a similar coordination sphere of the Mo ion that was recently assigned as a 6-sulfur coordinated Mo(V) species [24]. However, which and whether any of these Mo(V) species is actually involved in turnover is still ambiguous.

We have previously characterized, using protein film voltammetry (PFV) and EPR spectroscopy, the kinetics of a reductive activation in NapAB from *R. sphaeroides* [25]. This process is slow, irreversible and correlates with the disappearance upon reduction of the Mo-cofactor form that gives rise to the Mo(V) "high *g*" resting signal. However, the molecular mechanism underlying activation was unclear. In the present study, we show that the intramolecular electron transfer step from the [4Fe–4S] center to the Mo-cofactor is slow in the inactive Mo(V) "high *g*" resting state of the enzyme. We detect a spin–spin interaction between the Mo(V) species and the $[4Fe–4S]^{1+}$ cluster that is modified upon activation of the enzyme. This is interpreted as an activation process involving the pyranopterin chemistry: in the inactive "high *g*" resting Mo(V) species, the pterin proximal to the iron–sulfur center is fully oxidized to a non-functional pyran ring-opened form and is modified upon activation, while the first coordination sphere of the molybdenum ion does not change.

2. Material and methods

2.1. Cell cultures, purifications and activities assays

Samples of *R. sphaeroides f. sp. denitrificans* IL106 NapA, NapB and NapAB were purified as previously described [11].

2.2. Protein film voltammetry experiments

The electrochemical setup was the same as described in refs [25,26]. It consisted of a PGE rotating electrode, a SCE reference electrode and a platinum counter electrode. Before each measurement, the PGE electrode was abraded with alpha alumina (Buehler), sonicated, rinsed and dried. 0.6 μL of a 0.2 M neomycin sulfate solution was then deposited on the electrode, allowed to dry for 5 min. 0.6 μL of a stock solution of the *in vitro* reconstituted NapAB heterodimer (see below) was deposited. The electrolytic solution, buffered with (2-(N-morpholino)ethanesulfonic acid) MES, (N-cyclohexyl-2-aminoethanesulfonic acid) CHES, (2-[4-(2-hydroxyethyl)piperazin-1-yl]ethanesulfonic acid) HEPES, (3-[[1,3-dihydroxy-2-(hydroxymethyl)propan-2-yl]amino]propane-1-sulfonic acid) TAPS and sodium acetate (5 mM each), contained 0.1 M sodium chloride and 0.1 mM potassium nitrate.

2.3. In vitro reconstitution of the NapAB complex

NapAB dimer was reconstituted from independently purified NapA and NapB samples. NapA and NapB sample concentrations, determined by the Bradford method, were controlled spectrophotometrically by using the extinction coefficient of the iron–sulfur center in NapA ($\varepsilon = 21{,}200\ M^{-1}\ cm^{-1}$ at 400 nm) and of the reduced hemes in NapB ($\varepsilon = 280{,}000$, 41,000 and 66,000 $M^{-1}\ cm^{-1}$ at 419, 522 and 550 nm respectively) [14]. Based on the measured dissociation constant of 0.5 nM for the reduced heterodimer [11], we estimated that the complex would quantitatively form by adding 1 equivalent of a 400 μM NapB aliquot to NapA in order to obtain a NapAB sample at the concentration of about 80 μM. Control of the heterodimer formation was achieved by comparing the EPR signal of the hemes in native NapAB to that of the hemes in NapB before and after quantitative addition to NapA (Supplementary Fig. S1). Anchoring NapB to the NapA subunit induces a slight shift in the position of the low field EPR-line ($g_{1,2,3} = 2.97, 2.26, 1.48$ in NapB *versus* $g_{1,2,3} = 2.93, 2.27, 1.50$ in NapAB) and also a decrease of the *g*-strain, the EPR lines being narrower in the heme signal in both native and *in vitro* reconstituted heterodimers NapAB. Moreover, we observed that the Mo(V) "high *g*" resting signal remains the same both in shape and intensity in NapA before and after reconstitution of the NapAB heterodimer.

2.4. Low temperature EPR spectroscopy studies

The EPR spectra were recorded on a Bruker ELEXSYS E500 spectrometer fitted with an Oxford Instruments ESR 900 helium flow cryostat. Quantifications were made by using an external standard solution of freshly prepared 1 mM Cu-EDTA in 100 mM TRIS–HCl, 10 mM EDTA at pH8 transferred into a calibrated EPR tube.

2.5. Room temperature EPR spectroscopy studies

Room temperature EPR experiments were performed on an ESP300E Bruker spectrometer fitted with a variable temperature unit BVT3000 (Bruker) using liquid nitrogen as cryogen. The temperature inside the cryostat was controlled before and after each measurement using a temperature probe set in an EPR tube. For all experiments performed at room temperature, 70 μL of protein was kept into a quartz capillary tube. Kinetic experiments were performed by recording the EPR signal decay at fixed magnetic field as a function of time. 500 equivalents of sodium dithionite (20 μL at 100 mM) and 50 μL of a fresh Nap sample were mixed together in an anaerobic cell prior to quick transfer of 70 μL of the sample in a septum-sealed EPR capillary flushed with Ar. The capillary was subsequently placed into a cryostat-mounted resonator already cooled at a fixed temperature. The dead time in the kinetic experiments, including mixing, transfer of the protein in the capillary and the required time for the sample to stabilize at the regulated temperature in the cryostat, was about 3 min. Once the kinetic

measurement was achieved, the complete extinction of the Mo(V) signal was checked by recording a room-temperature spectrum and the redox status of the sample in the capillary was controlled by low temperature EPR spectroscopy. We ensured that no magnetic field drift occurred during the course of the experiment (up to 2 h).

2.6. Preparation of the Mo(V) species

The Mo(V) "high *g*" resting form was detected in all *R. sphaeroides* NapA and NapAB aerobically-purified samples studied so far. The "high *g*" species is stable at room temperature under both aerobic and anaerobic conditions. In these samples, the iron–sulfur and heme centers are oxidized. The "high *g*" species can be detected together with the reduced $[4Fe–4S]^{1+}$ center by freezing a NapA sample incubated with about 100 equivalents of dithionite for less than 1 min at room temperature (all sodium dithionite solutions were prepared just before use from Ar-degassed powder dissolved in the protein buffer, 20 mM Hepes pH 8, 50 mM NaCl). Two procedures were used to prepare the "high *g* nitrate" Mo(V) form in NapA and NapAB, the proportions of which did not exceed 0.15 spin/protein in our experiments. In the first procedure, the "high *g* nitrate" state was obtained by adding nitrate (from 100 to 150 mM final concentration) to a sample (25 to 80 μM of protein) that was firstly reduced with 100 equivalents sodium dithionite (5–10 mM final concentration). We checked using low temperature EPR that the "high *g*" resting signal had totally vanished before re-oxidizing the sample with nitrate. In the second procedure, the sample was first activated by incubation with 500 equivalents dithionite for 1 h. The sample was then reoxidized by exposure to air, washed under aerobic conditions with a final buffer consisting of 100 mM MES, 50 mM NaCl at pH 6 or 50 mM HEPES pH 8, 50 mM NaCl. Under these conditions, the reoxidized sample was EPR-silent and the Mo(V) "high *g* nitrate"-like signal developed by further reduction with 200 equivalents of dithionite. In all sample preparations showing the "high *g* nitrate", both the iron–sulfur cluster and the hemes (in NapAB only) were reduced.

3. Results

3.1. Slow decay of the Mo (V) "high g" EPR signal under reductive conditions

Air-purified samples of NapAB display at 15 K an EPR signature at $g = 2.93, 2.27, 1.50$ associated to the two low spin $S = 1/2$ *c*-type hemes of the NapB subunit (Fig. 1c). In addition to the heme signal, a slow relaxing signal is visible around $g \sim 2$. This rhombic signal is better observed at higher temperature (55 K in Fig. 1e) and is due to a paramagnetic Mo(V) $S = 1/2$ species with *g*-values at 1.999, 1.991, 1.981 (Table 1). This signal shows hyperfine interaction with two non-exchangeable $I = 1/2$ nuclei, attributed to the β-methylene protons of the cysteine that binds the molybdenum ion [21]. The average *g*-value of this Mo(V) signal is higher than usual for Mo(V) EPR signals; for this reason the Mo(V) species have been called "high *g*". Among them, the "high *g*" resting form, that is observed in the *as purified* enzymes, is identical in both *R. sphaeroides* NapA and NapAB samples except that it accounts for 30–60% of the enzyme in NapA and 5–20% in NapAB, depending on the purification batch. In the air-purified NapAB,

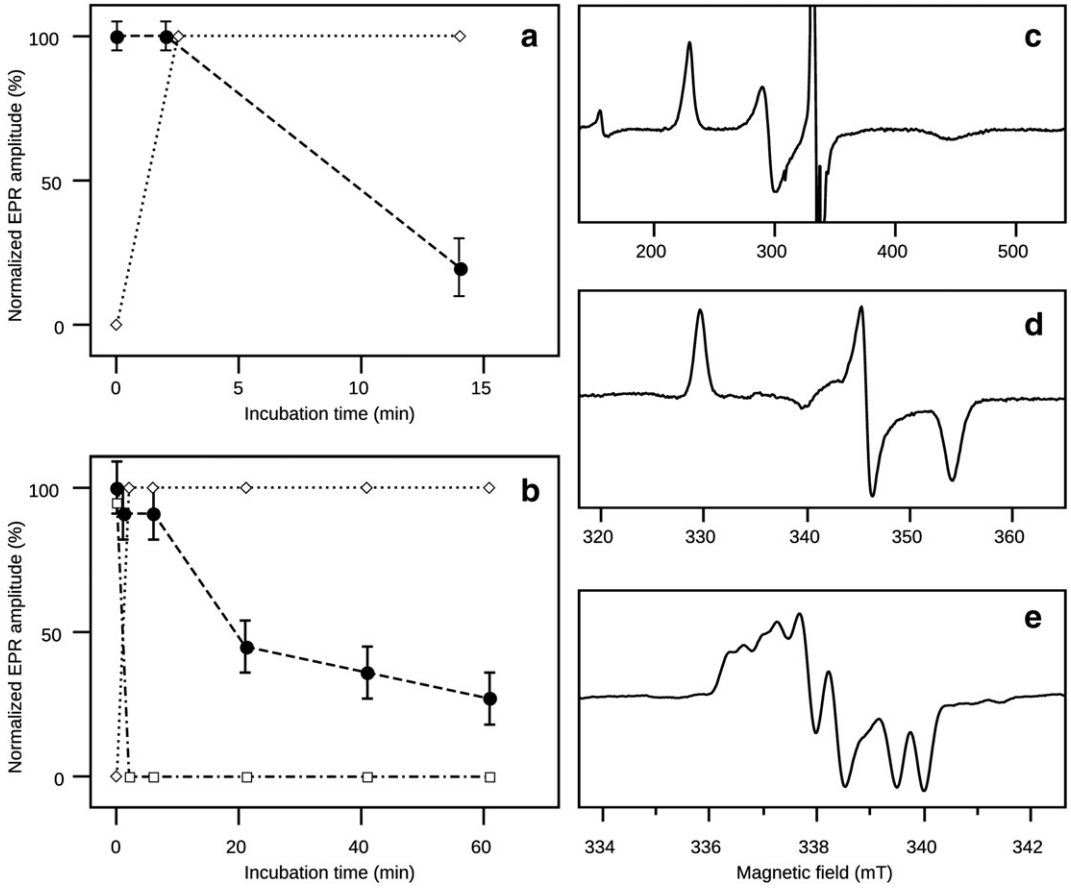

Fig. 1. EPR signatures of the redox centers in *Rhodobacter sphaeroides* NapAB and signals decay over incubation time with dithionite at room temperature monitored by low temperature EPR in NapA and NapAB. Left panels- Evolution of the EPR signal amplitude of the "high *g*" Mo(V) species (●), $[4Fe–4S]^{1+}$ (◇) and hemes (□) in NapA (a) and NapAB (b) upon addition of 100 equivalents of sodium dithionite. Right panels - EPR signatures of the *c*-type hemes (c), $[4Fe–4S]^{1+}$ center (d) and the Mo(V) "high *g*" species (e) in NapAB. EPR recording conditions: microwave frequency 9.408 GHz (a) temperature 15 K, modulation amplitude 2 mT, microwave power 4 mW; (b) 15 K, 0.5 mT, 1 mW; (c) 55 K, 0.2 mT, 1 mW.

Table 1
g- and *A*-parameters for the Mo(V) "high *g*" species in *Rhodobacter sphaeroides* NapA and NapAB. The parameters given are those determined in the simulations of the experimental EPR-spectra by using the EasySpin package [28]. n.d.: not determined.

Mo(V) 'high *g*' species	*g*-values (g_1, g_2, g_3)			g_{av}	$g_{anisotropy}$ (g_1–g_3)	Rhombicity (g_1–g_2)/(g_1–g_3)	Hyperfine splitting *A*/gβ (mT) (A_1, A_2, A_3)			Reference
High *g* resting NapAB	1.9989	1.9908	1.9812	1.9903	0.0177	0.458	0.61	0.56	0.50	[27]
							0.29	n.d.	n.d.	
High *g* resting NapA	1.9988	1.9909	1.9812	1.9903	0.0176	0.449	0.64	0.52	0.50	This work
							0.29	n.d.	n.d.	
High *g*-reduced $[4Fe–4S]^{1+}$ NapA	1.9983	1.9911	1.9811	1.9902	0.0172	0.419	0.62	0.51	0.49	This work
							0.29	n.d.	n.d.	
High *g* nitrate NapA	1.9977	1.9886	1.9813	1.9892	0.0164	0.555	0.57	0.47	0.45	This work
							0.26	n.d.	n.d.	

an additional species at $g = 2.02$, 2.00 and 1.99, referred to "very high *g*" in the literature, is sometimes visible together with the "high *g*" species (not shown). In our preparations, the "very high *g*" form never exceeded 0.05 spin/protein. The third type of Mo(V) signal, called "low *g*", is only occasionally observed in dithionite-reduced samples of Nap from *R. sphaeroides* (not shown).

Upon addition of an excess of sodium dithionite to an air-purified sample of NapAB, followed by a short incubation time (less than 1 min) and by freezing in liquid nitrogen, the signal of the hemes disappears and a signal typical of a $S = 1/2$ reduced $[4Fe–4S]^{1+}$ cluster is detected at $g = 2.04$, 1.95, 1.90 (Fig. 1d). The same signal is observed for NapA which has no hemes. Surprisingly, the intensity of the "high *g*" Mo(V) signal remains unchanged after incubation with dithionite for a few minutes. We monitored the disappearance of the "high *g*" resting signal incubated with the reductant by low temperature EPR (Fig. 1). To do so, the sample was quickly thawed under Ar atmosphere and refrozen after different incubation times. The total extinction of the Mo(V) "high *g*" resting signal occurred in less than 20 min for NapA (Fig. 1a) and more than 1 h for NapAB (Fig. 1b). This slow reduction of the "high *g*" resting form has already been observed in *P. pantotrophus* NapAB [2,20]. Furthermore, once extinguished, this signal cannot be regenerated by oxidation of the sample with ferricyanide or air, whereas the other cofactors show a fully reversible redox behavior [25]. This suggests that the redox properties of the Mo-cofactor are modified by the enzyme activation process. In addition, in NapAB samples in which a "very high *g*" Mo(V) signal could be detected together with the "high *g*" signal, the former disappeared as quickly as the heme signal upon reduction (not shown), suggesting that the slow decay of the Mo-cofactor is a peculiar feature of the "high *g*" resting form.

3.2. Kinetic study of the Mo(V) "high *g*" signal extinction monitored by EPR spectroscopy at room temperature

Due to its slow relaxation properties, the "high *g*" resting signal can still be observed at room temperature, as shown in Fig. 2. The position and shape of the EPR lines indicate that the tumbling of the protein is slow enough not to average (or to average only weakly) the **g**- and **A**-tensors anisotropy of the EPR species. Room temperature EPR Mo(V) signals have been reported in a few molybdo-proteins, but the advantages of detecting Mo(V) signals in fluid protein solution have been rarely exploited [29–31]. Here the kinetics of the "high *g*" Mo(V) EPR signal decay after anaerobic addition of 500 equivalents of sodium dithionite were monitored in NapA, and in the native and *in vitro* reconstituted NapAB heterodimers. These EPR experiments are very demanding in terms of amount of biological material since, once reduced, the "high *g*" resting state cannot be restored. The evolution of the EPR signal amplitude as a function of the incubation time with the reductant is shown in Fig. 3. The experimental data can be described by a monoexponential decay giving apparent time constants of 2.8 ± 0.2 min for NapA, 21 ± 3 min for NapAB and 18 ± 1 min for the reconstituted NapAB complex, all at room temperature (ca. 23 °C). The corresponding pseudo-first-order rate constants (called k_{dec} for decay) are reported in Table 2. The extinction of the "high *g*" signal is about 6 times faster for NapA than for the NapAB complex. This shows that the rate of Mo(V) signal decay is affected by the presence of the NapB subunit, as previously shown for the rate of reductive activation by PFV [25]. Adding low potential redox mediators, either methyl viologen or a mixture of mediators, at 10% of the protein concentration had no noticeable effect on the kinetics of the Mo(V) signal extinction (Table 2). The temperature dependence of the reduction process of the Mo(V) "high *g*" resting state was also investigated on NapA to take advantage of the higher relative proportion of the "high *g*" resting signal than in NapAB. Fig. 4 shows the results as an Arrhenius plot, from which an activation energy value of 69 ± 8 kJ/mol can be derived.

3.3. Comparison of kinetic parameters for the reductive activation studied by PFV and by EPR

We compared the effect of temperature on the rate of activation of NapA, measured using EPR, and of NapAB, measured using electrochemistry, since NapAB gives more intense electrochemical signals than NapA. In a previous electrochemical study, we showed that films of periplasmic nitrate reductase undergo a slow activation process the first time the enzyme is poised at a sufficiently low potential [25]. This reductive activation is illustrated in the chronoamperogram of Fig. 5b, obtained with a fresh film of NapAB adsorbed onto a rotating graphite electrode, and immersed into a solution of 0.1 mM nitrate, when the electrode potential is changed as indicated in panel a (Fig. 5). The magnitude of the current is proportional to turnover rate (the more negative

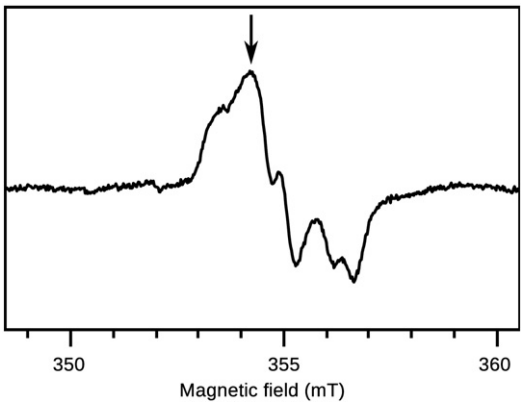

Fig. 2. EPR signature of the Mo(V) "high *g*" resting species at room temperature in *Rhodobacter sphaeroides* NapA. Enzyme concentration about 100 μM, the "high *g*" Mo(V) represents about 0.3 spin per protein. EPR recording conditions: microwave frequency 9.879 GHz, modulation amplitude 0.2 mT, microwave power 8 mW. Arrow marks the position of the magnetic field chosen for kinetic measurement at room temperature (on Fig. 3).

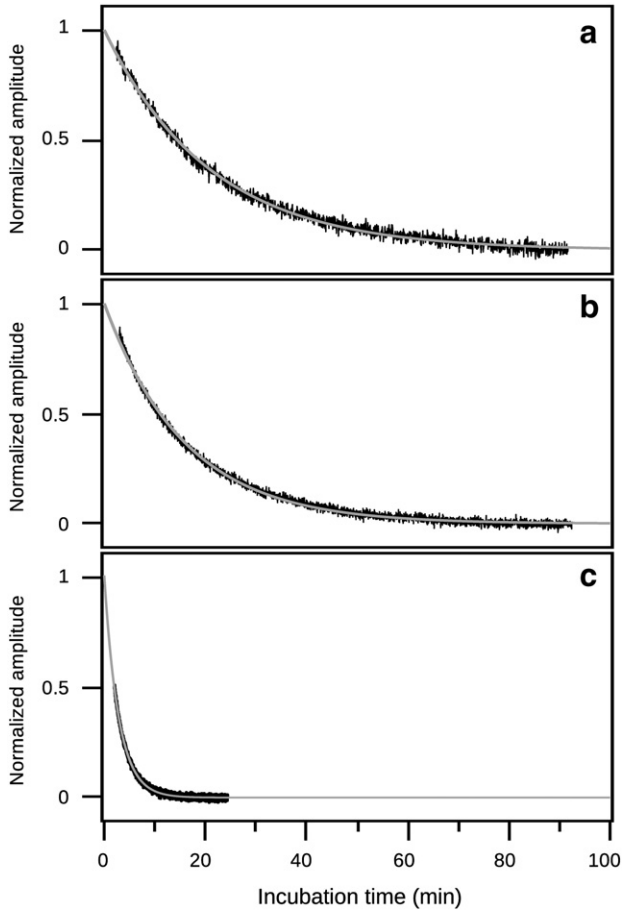

Fig. 3. Kinetics of reduction of the Mo(V) "high *g*" resting species monitored by EPR at fixed magnetic field and room temperature (23 °C). Traces a), b) and c) correspond to reduction in native NapAB complex, *in vitro* reconstituted NapAB complex and NapA respectively, at pH 8. Position of the magnetic field is marked by an arrow on Fig. 2. Experimental decays in traces a, b and c are adjusted with monoexponential fits (gray lines) with time constants τ: 21 min (native NapAB), 18 min (reconstituted NapAB) and 2.8 min (NapA).

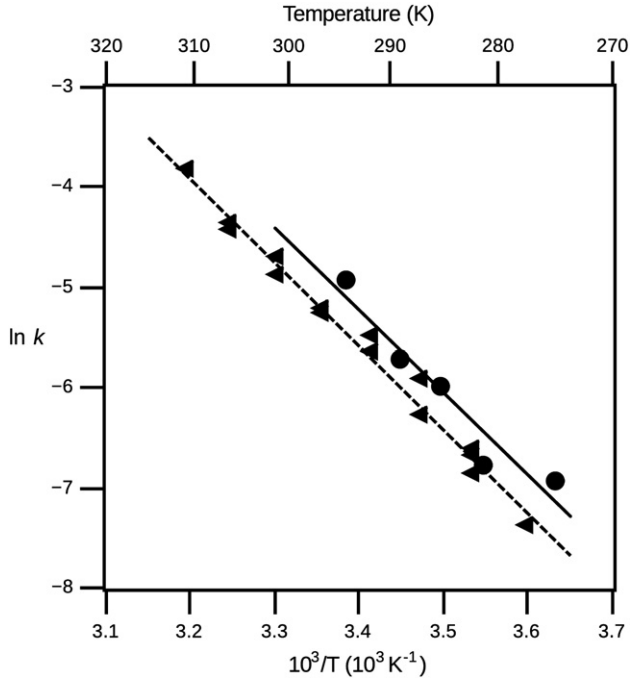

Fig. 4. Temperature dependence of the apparent kinetic rate constants for the decay of the Mo(V) "high *g*" resting signal monitored by EPR at room temperature (k_{dec}, ●) and of the irreversible reductive activation process studied by PFV (k_{act}, ▲). EPR experiments were performed on NapA at pH8 (in the presence of 10 μM methyl viologen) and PFV experiments on NapAB at pH6.

the current, the higher the activity). When the potential is poised at $E = -160$ mV (at $t = 1$ min), the current is essentially constant. On the step to −460 mV, at $t = 4$ min, the activity first instantly decreases (the current becomes less negative), consistent with the lower activity at lower potentials [32] and then slowly increases before it stabilizes. This slow change in current demonstrates that the enzyme activates at low potential. When this sequence of potential steps is repeated with the same film of enzyme, after a poise at +240 mV (from $t = 46$ min), the activity detected at $E = -160$ mV is greater than that measured on the first step at this potential (at $t = 1$ min), and no further activation occurs on the second step to −460 mV, at $t = 51$ min. Therefore, the activation proceeds only once, on the first step to −460 mV, and it is not reversed by taking back the enzyme to oxidizing conditions (+240 mV), indicating that the enzyme inactivation is a very slow process.

We have shown before that the relative magnitude of this activation equates the fraction of Mo(V) "high *g*" resting that is present in the sample before activation [25]. We concluded that this species is an inactive form that irreversibly activates the first time the enzyme is reduced. In order to mirror the kinetic measurements made with EPR, we have used electrochemistry to investigate the temperature dependence of the activation rate constant k_{act} with NapAB at pH 6. The data summarized in Table 2 show a five-fold difference between the rate constants measured at pH 8 and 6 in two completely independent experiments (PFV versus EPR). The fact that this difference is small is consistent with our former conclusion that the rate of the activation process depends only very weakly on pH [25]. From the data in Fig. 4, we calculated an activation energy value of 69 ± 5 kJ/mol. The agreement between data derived from chronoamperometry and room temperature EPR experiments shows that the reduction of the Mo(V) "high *g*" resting into Mo(IV) and the activity enhancement seen by electrochemistry depend on the same rate-determining step.

Table 2
Rate constants of the reductive activation and reduction potential of the redox centers in *R. sphaeroides* NapA and NapAB.

	Reduction rate of the Mo(V) "high *g*" k_{dec} (s^{-1}) from EPR experiments at 23 °C, pH8	Activation rate k_{act} (s^{-1}) from PFV experiments, at 25 °C, pH6	Redox potential $E^{o'}$ (Mo^{V}/Mo^{IV}) (mV *vs* SHE) at pH7	Redox potential $E^{o'}$ $[4Fe\text{–}4S]^{2+/1+}$ (mV *vs* SHE) at pH 7
NapA	$6.5\ 10^{-3}$	$2.6\ 10^{-2}$ [b]	−210 mV[c]	−240 mV[c]
Native NapAB	$8\ 10^{-4}$	$6\ 10^{-3}$ [b]	−225 mV[c]	−80 mV[c]
Reconstituted NapAB	$9.5\ 10^{-4}$ (11.10^{-4} with mediators[a])	$5.4\ 10^{-3}$	n.d.	n.d.

a: in the presence of mediators (ferrocene monocarboxylic acid, potassium hexacyanoferrate(III), 2,6-dichlorophenol-indophenol, 2,5 dimethyl-*p*-benzoquinone, 1,2-naphtoquinone, phenazine methosulfate, phenazine ethosulfate, methylene blue, resorufin, indigo carmine, 2-hydroxy-1,4-naphtoquinone, phenosafranine, neutral red and methyl viologen, 3 μM final each), b: reference [25], c: reference [11].

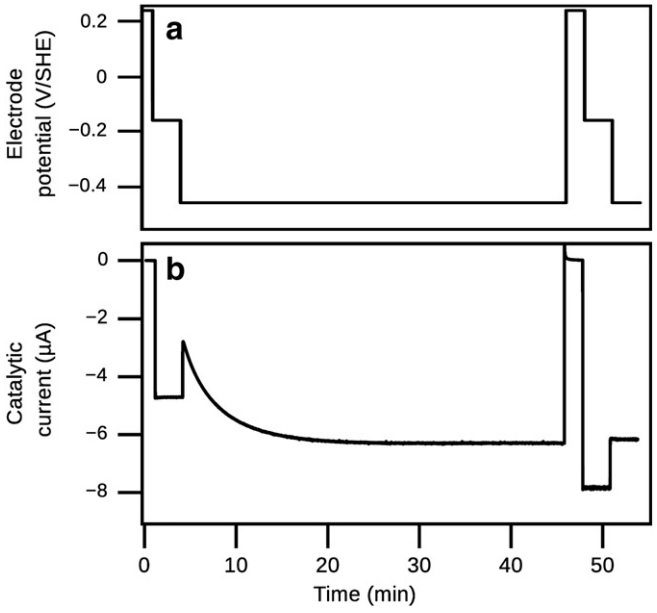

Fig. 5. Chronoamperometric experiment evidencing the irreversible activation process occurring during the first reduction of *in vitro* reconstituted NapAB. Electrode rotation rate 5000 rpm, pH 6, 20 °C. Data have been corrected for film desorption as described in reference [33].

3.4. Modification of the spin–spin interactions between the Mo center and the [4Fe–4S]$^{1+}$ cluster upon reductive activation

The shape of the Mo(V) "high *g*" resting EPR signal detected in frozen samples of *as prepared* Nap is independent of temperature, as observed up to 240 K and illustrated at 15 and 80 K (Fig. 6a, b). Upon reduction with dithionite followed by rapid freezing, the [4Fe–4S] becomes fully reduced and paramagnetic (S = 1/2) while the "high *g*" Mo(V) signal remains observable. The latter is shown at 80 K and 15 K in traces 6c and 6d. At 80 K, the Mo(V) EPR spectrum shows no significant changes in *g*- and *A*-values upon reduction of the proximal [4Fe–4S] (see Table 1). In contrast, weak spin–spin interactions between the "high *g*" Mo(V) and the reduced iron–sulfur center develop at 15 K as additional lines-splitting (Fig. 6d); the magnitude of the interaction (about 0.5 mT) is similar to the hyperfine splitting (Table 1). Spin–spin interactions are visible on the EPR spectrum at temperatures up to 40 K at which the [4Fe–4S]$^{1+}$ signal disappears due to relaxation broadening.

Once the enzyme fully reduced and activated, we can detect another Mo(V) species both in NapA and NapAB by adding an excess of nitrate (see material and methods for details). Such species was originally observed in reduced *A. vinelandii* nitrate reductase in the presence of an excess of nitrate and later called "high *g*" nitrate [8,20]. In *R. sphaeroides* nitrate reductase, the "high *g* nitrate" Mo(V) can also be produced in the absence of nitrate after a redox cycling procedure, which consists of a reductive activation followed by air-oxidation and then reduction with dithionite. The "high *g* nitrate" displays *g*-values and ^{1}H-hyperfine couplings that are close but slightly different from those of the "high *g*" resting species (compare traces a and e in Fig. 6, and see Table 1). The two "high *g* nitrate" forms observed with or without nitrate present the same continuous-wave EPR features and line splitting. In all samples prepared, the Mo(V) "high *g* nitrate" was detected with the iron–sulfur cluster being in the reduced state. The "high *g* nitrate" EPR spectra presented in Fig. 6e (80 K) and 6f (15 K) come from a sample obtained without nitrate. As for the "high *g*" signal, the line splitting due to magnetic coupling with the [4Fe–4S]$^{1+}$ center disappears above 40 K. We observed that at 15 K, the pH value (6 or 8) had an influence neither on the shape nor on the splitting of the Mo(V) signal (not shown). At 15 K, the spectrum of the Mo(V) "high *g* nitrate" species coupled to the iron–sulfur cluster shown in Fig. 6f is characterized by a splitting of the g_1 and g_2 lines and a slight broadening of the g_3 lines.

Whereas "high *g*" resting and "high *g* nitrate" species display close *g*- and *A*-values, the overall comparison of the two split signals at 15 K evidences significant changes in the spin–spin interactions after reductive activation. The most visible modification is that the g_3-lines are split in the "high *g*" resting but not in the "high *g* nitrate" states (compare Fig. 6d and f). However, the magnitude of the splitting does not significantly change between both "high *g*" Mo(V) species. Similar weak spin–spin interactions between the Mo-cofactor and the

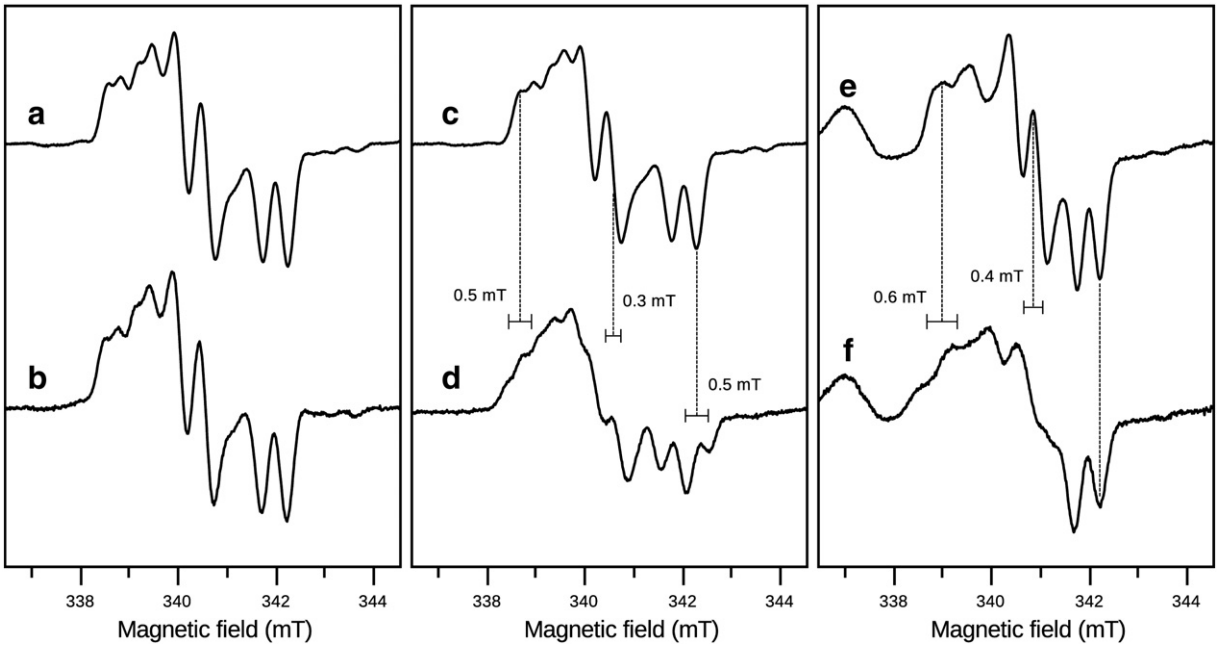

Fig. 6. EPR signatures of the Mo(V) "high *g*" resting- oxidised [4Fe–4S]$^{2+}$, "high *g*"- reduced [4Fe–4S]$^{1+}$ and "high *g* nitrate"- reduced [4Fe–4S]$^{1+}$ species at 80 K (a, c, e) and 15 K (b, d, f) in *Rhodobacter sphaeroides* NapA. All spectra presented here were obtained with NapA (concentration 70–80 μM) at pH8 (a–d) and pH6 (e–f). EPR recording conditions: microwave frequency ν = 9.48GHz, modulation amplitude 0.1 mT, modulation frequency 100 kHz; a), c), e) temperature 80 K, microwave power 1 mW; b) 15 K, 1 μW; d) 15 K, 3 μW and f) 15 K, 10 μW.

adjacent Fe–S cluster have been described in other molybdoenzymes such as xanthine oxidase (XO) [34] or aldehyde oxidoreductase (AOR) [35]. In these proteins, magnetic interactions between various Mo(V) species and the proximal $[2Fe–2S]^{1+}$ center are visible by EPR at low temperature, with lines splitting of the Mo(V) signals ranging from about 0.5 to 2.5 mT [34,36]. Quantitative studies of the magnetic couplings between the Mo(V) species and the proximal $[2Fe–2S]^{1+}$ (at 16 Å from the Mo ion in AOR, and 19 Å in XO) showed that the contributions from dipolar and exchange interactions are comparable, with exchange parameter values deduced from spectrum analysis of $J = 1.2 \times 10^{-3}$ cm^{-1} for AOR [37] and 2.2×10^{-3} cm^{-1} for XO [34] (with the convention for the exchange term $+ J\mathbf{S}_A.\mathbf{S}_B$). In *R. sphaeroides* NapAB, the distance between the Mo ion and the [4Fe–4S] center (taken at the center of the iron tetrahedron) is close to 13.5 Å according to the crystal structure. With such a distance, comparable contributions (of about 10^{-3} cm^{-1}) from the dipolar and exchange interactions to the spin–spin coupling are expected, which is consistent with the Mo(V) signal line splittings observed at low temperature.

4. Discussion

4.1. Fast intramolecular electron transfer between the iron–sulfur center and the Mo-cofactor is recovered upon reductive activation

A reductive activation process has been observed for several nitrate reductases: the membrane-bound *E. coli* NarGH [38], the soluble cytoplasmic *S. elongatus* Nas [38] and the periplasmic *R. sphaeroides* Nap [25]. This reductive activation has been evidenced in protein film voltammetry experiments by a slow increase of the catalytic current the first time the potential of the electrode is stepped down (Fig. 5). In *R. sphaeroides* NapAB, we have previously shown that this process is slow, pH- and nitrate concentration-independent, irreversible and related to the disappearance of the Mo-cofactor form that gives rise to the Mo(V) "high *g*" resting signal [25]. This species is observed in variable amounts in as-prepared samples of Nap: about 10–20% in NapAB and up to 60% in NapA.

Here, we have demonstrated that reductive activation includes the slow reduction of the Mo(V) "high *g*" resting form, the others redox centers of the protein being quickly reduced by dithionite on the time scale of our experiments. Kinetic experiments performed by room-temperature EPR spectroscopy enabled us to measure the pseudo-first order rate constant of decay (k_{dec}) of the "high *g*" resting signal. This constant is independent of the presence of methyl viologen or a cocktail of mediators, but it is lower when the catalytic subunit NapA is associated to NapB ($k_{dec,\ NapA}/k_{dec,\ NapAB} \sim 6$, see Table 2). This ratio is consistent with the rates of the first activation measured by PFV, which are four times faster in NapA than in NapAB [25]. We have studied the effect of the temperature on the rate of activation by EPR with NapA, and by electrochemistry with NapAB, and have determined the same activation energy $E_a = 69$ kJ mol^{-1}.

Intramolecular electron transfer between FeS and the Mo-cofactor must be slow in the inactive enzyme since the iron–sulfur in NapA (and the hemes in NapAB) are quickly reduced whereas the "high *g*" Mo(V) signal requires minutes to hours to completely vanish. If we suppose that the rate-limiting step in the activation process is precisely the intramolecular electron transfer step from the $[4Fe–4S]^{1+}$ to the Mo-cofactor, then the apparent rate constants k_{dec} or k_{act} can be interpreted by using the Marcus equation (Eq. (1)):

$$k_{ET} = \frac{2\pi}{\hbar}\frac{\left|T_{ab}^2\right|}{\sqrt{4\pi\lambda k_B T}}\exp\left(\frac{-(\Delta_r G^\circ + \lambda)^2}{4\lambda k_B T}\right) \quad (1)$$

At room temperature, the $T^{-1/2}$ term is of little influence, so that the exponential term can be expressed as the function of the activation energy determined experimentally. The free enthalpy of reaction $\Delta_r G^\circ$ can be roughly estimated using the redox potentials derived from potentiometric titrations coupled to EPR spectroscopy for the Mo(V)/Mo(IV) and $[4Fe–4S]^{2+/1+}$ transitions for NapA and NapAB at pH 7 (Table 2). This gives a free energy $\Delta_r G^\circ = RT\,(E^\circ_{4Fe} - E^\circ_{Mo}) \sim -30$ meV and -145 meV for NapA and NapAB, respectively, which can be reasonably neglected with respect to the reorganization term λ. Indeed, using the activation energies determined above, one deduces that $\lambda \sim 4E_a = 2.8$ eV for both NapA and NapAB. With such values of λ, the ratio of activation rates constant between NapA and NapAB can be explained by a slightly different electronic coupling matrix element T_{ab} of 5.6 cm^{-1} and 1.6 cm^{-1} for NapA and NapAB respectively. The unreasonably high value of the reorganization energy λ is not consistent with a pure electron transfer reaction. This rather suggests that the electron transfer depends on a chemical step that precedes it, a mechanism described as a gated or coupled electron-transfer in the literature [39,40].

Alternatively, the intramolecular electron transfer may be extremely slow in the inactive enzyme, even slower than the measured activation rate. The reductive activation would then require that dithionite directly reduces the Mo-cofactor, either from the surface through the more solvent-exposed pyranopterin, or after diffusion towards the active site along the substrate access channel. The formation of the NapAB complex may slightly modify the structure of the channel and the accessibility of the Mo-cofactor, thus explaining the changes in activation rate between NapA and NapAB. However, we consider this mechanism as unlikely since direct electron transfer from the working electrode to the Mo-cofactor is impossible in electrochemical experiments.

The observation that the "high *g*" resting EPR signal slowly decays is apparently conflicting with the former kinetic model we proposed, in which the activation proceeded by fast (Nernstian) reduction of the Mo(V) ion followed by a slow and irreversible chemical step [25]. All kinetic data can however be rationalized in a refined model by considering that a slow and rate-limiting equilibrium transformation at the Mo-cofactor in the Mo(V) state precedes the reduction to the Mo(IV) state.

4.2. A molecular model of reductive activation

No molecular mechanism of reductive activation in Nap has been proposed so far. We have previously shown that this activation is not reversed under any of the conditions tested in our experiments (exposure to concentrated HEPES or MES buffers, Ni^{2+}, Zn^{2+} with or without nitrate, sulfite, sulfide, azide, imidazole, glycerol, O_2, or electrode potentials up to +640 mV for up to 5 min) [25]. This suggests that the inhibition is probably not due to an exogenous molecule that enters the molybdenum coordination sphere.

Once the enzyme fully reduced and activated, we detect in certain conditions another EPR-active Mo(V), previously named in the literature "high *g* nitrate". Its *g*-values are very close to those from the "high *g*" resting, with slight changes in the ^{1}H-hyperfine couplings. This shows that the reductive activation does not involve significant modifications in the first coordination sphere of the Mo ion. However, the "high *g* nitrate" species displays a spin–spin interaction spectrum which is different from the one observed for the inactive Mo(V) "high *g*" resting state thus reflecting some structural modifications between the Mo^{5+} ion and the $[4Fe–4S]^{1+}$ (Fig. 6).

Spin–spin interactions between paramagnetic centers may be affected by the modification of either the dipolar or the exchange magnetic interactions, or both. The electronic structures of both the Mo(V) and $[4Fe–4S]^{1+}$ being unchanged, the dipolar component of the magnetic interaction would be modified only if the relative arrangements of the Mo and [4Fe–4S] centers were modified, which is unlikely. We therefore favor the possibility that the exchange coupling pathway between centers is changed upon activation, which modulates the magnitude of the exchange coupling constant. Such an interaction depends on the overlap between the magnetic molecular orbitals of the interacting

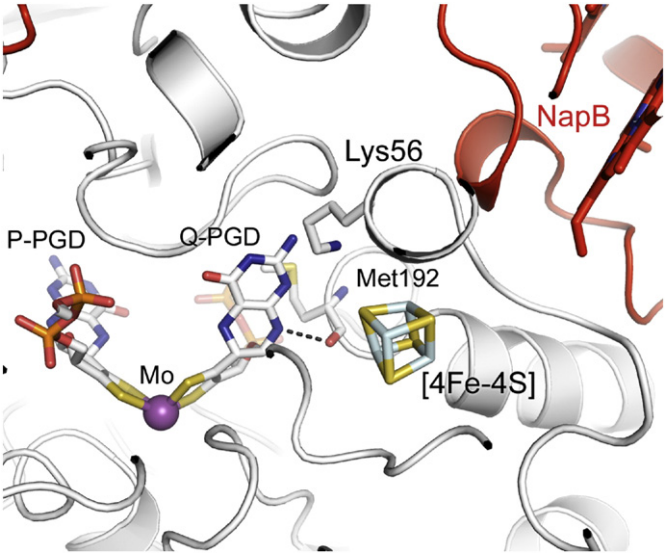

Fig. 7. Zoom on the molybdenum cofactor and the [4Fe–4S] cluster in *Rhodobacter sphaeroides* NapAB (PDB code: 1OGY).

paramagnetic centers. Based on available Nap crystal structures, we propose an exchange coupling pathway between the Mo ion and the [4Fe–4S] involving lysine 56 and the pyranopterin proximal to the iron–sulfur cluster (Q-PGD in Fig. 7). Chemical modifications of the proximal pyranopterin, such as a conformational and/or redox changes, would precisely affect the exchange coupling pathway between the Mo-cofactor and the [4Fe–4S] cluster.

Although pterins can exist in a variety of redox states, pyranopterins are thought to be present in either the "dihydro" or the "tetrahydro" reduced forms in molydboenzymes (Fig. 8) [41]. In Mo-bisPGD enzymes, the conformation of the pyranopterin proximal to the iron-sulfur center would be consistent with the tetrahydro state and the distal pyranopterin with a dihydro conformation [41]. Furthermore, in most of the available crystal structures, pterins present a tricyclic structure with a pyran ring fused to the pyrazine ring of the pterin unit. A bicyclic pyran ring-opened form has been observed in two crystal structures from the Mo-bis-PGD enzymes family, namely the heterotrimeric membrane-bound nitrate reductase (NarGHI) from *E. coli* and *Aromatoleum aromaticum* ethylbenzene deshydrogenase EdbH [42,43]. Several authors propose the participation of scission/condensation reactions of the pyran ring in catalysis at the metal center [41,44–46]. Another point is whether the pterin redox reactivity is involved in the catalytic reaction of the enzymes [45,46]. These two aspects are difficult to address, especially because of the *in vitro* instability of the pyranopterin upon release from the protein. Nevertheless, one can learn from *in vitro* studies about the reactivity on pyranopterin and molybdopterins complex. Thus, several studies have shown the reversibility of the pyran-cycle formation [47], or that pyranopterin oxidation leads to the bicyclic oxidized pterin (Fig. 8, form 4) [48,49].

Relying on this literature, we propose that the Mo(V) "high *g*" resting form in *R. sphaeroides* NapAB is inactive because the proximal pterin ligand of the Mo-cofactor is present in a fully oxidized and ring-opened form (form 4 in Fig. 8), impeding efficient intramolecular electron transfer. The variations observed in the low-temperature EPR spectrum of the Mo(V) species, before and after activation, interpreted as a modification of the proximal pyranopterin affecting the exchange coupling pathway, support this hypothesis. In the inactive enzyme, the oxidized and open state of the pterin affects the reduction potential of the Mo(V)/Mo(IV), as evidenced by the fact that Mo(V) has a large potential stability range before the activation while it is not detectable afterwards [25,50]. Such thermodynamic influence was discussed in the case of sulfite oxidase, which undergoes inhibition upon oxidation of the pyranopterin cofactor by ferricyanide [51]. Even though oxidized sulfite oxidase retains some activity, electron transfer from the molybdenum site is severely slowed. This led to two main hypotheses with regard to the role of the pyranopterin in sulfite oxidase activity, either acting as an electron transfer conduit or modulating the molybdenum reduction potential, the latter being favored on the basis of spectroscopic studies on synthetic models which mimic the ferricyanide-inhibited sulfite oxidase Mo-cofactor [52]. In periplasmic nitrate reductase, the reduction of the pterin and the formation of the pyran ring probably modify both the thermodynamic properties of the Mo ion and the kinetics of the electron transfer, thus enabling recovery of physiologic intramolecular electron transfer between the [4Fe–4S] center and the Mo ion.

The overall mechanism of the reductive activation we propose, presented in Fig. 9, includes the cyclization of the pyran unit and the two-electron and two-proton reduction of the proximal pterin, yielding the tetrahydropyranopterin state (form 1, Fig. 8). A more detailed mechanism requires considering the source of the electrons needed to

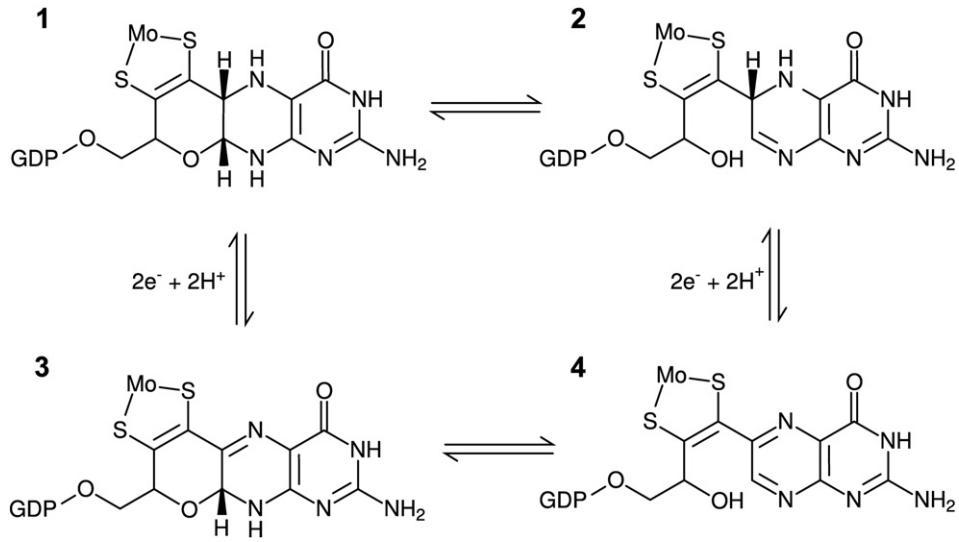

Fig. 8. Representations of the pyranopterin ligand in the "dihydro" (3) or the "tetrahydro" (1) tricyclic states. The equilibrium between the forms 1 and 2 (one of the possible tautomer is represented here), or 3 and 4, corresponds to condensation/scission reaction of the pyran ring.

Fig. 9. Proposed overall molecular mechanism for the irreversible activation occurring upon reductive treatment of the *as prepared R. sphaeroides* NapAB (or NapA) in the Mo(V) "high *g*" resting state. Irreversible conversion of the inactive into a catalytically competent form of the enzyme includes the formation of the pyran ring and the 2-electron, 2-proton reduction of the fully oxidized pterin to the functional tetrahydropyranopterin state.

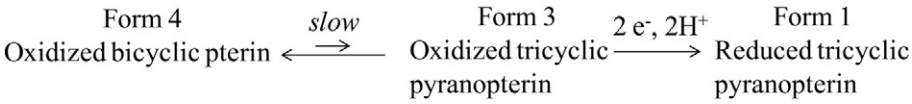

Scheme 1. Putative mechanism for the reductive activation centered on the proximal pterin of the Mo-cofactor of periplasmic nitrate reductase.

reduce the pterin, and whether the formation of the pyran unit precedes the reduction of the pterin or not. Studies on synthetic pyranopterins reactivity have shown that air (or ferricyanide) oxidation yielded the oxidized bicyclic pterin (form 4), that is then thermodynamically more stable than the oxidized tricyclic counterpart (form 3 in Fig. 8) [45,49]. Considering that the equilibrium between forms 4 and 3 is strongly shifted towards form 4, we favor the mechanism presented in scheme 1, in which the slow and reversible formation of the pyran ring that produces the dihydro state (form 3) constitutes the first step. This would be followed by the irreversible reduction of the pterin to form the tetrahydropyranopterin form (form 1), locking it in the tricyclic form. The latter step may become mostly irreversible for thermodynamic reasons, especially if the reduction potential of the pterin is significantly higher than that of the redox center providing/removing the electrons.

We have concluded above that the electrons necessary to reduction of the pterin moiety transit through the [4Fe–4S] center. Two possible mechanisms can be envisioned. In a first mechanism, the [4Fe–4S] center would deliver the two electrons to the pterin moiety one at a time (but only when the pyran ring is formed). This reduction would be the rate-limiting step of the reactivation. Once the pterin is closed and reduced, fast electron transfer can occur between the [4Fe–4S] and the molybdenum, in the normal catalytic cycle. In an alternative mechanism, electron transfer between the [4Fe–4S] and the molybdenum would be recovered at least partially when the pterin is oxidized and closed: the reduction of molybdenum ion would be slow because it is gated by the conformational change of the pterin (formation of the pyran ring). Once the molybdenum is reduced to the IV state, the transfer of two electrons from the molybdenum would reduce the pterin and lock it in the tricyclic form.

4.3. Conclusions

In this paper, we conclude that the mechanism of the reductive activation in *R. sphaeroides* NapAB does not involve the first coordination sphere of the Mo ion but the pyranopterin that is proximal to the [4Fe–4S] center. Based on magneto-structural correlations, we have recently proposed that the Mo(V) "high *g*" species in soluble nitrate reductases corresponds to a six-sulfur coordinated molybdenum ion [24], as seen in the recent high resolution crystal structure of NapAB from *C. necator* [14]. This suggests that a six-sulfur coordinated Mo^V species could be an intermediate involved in turnover. Such catalytically competent Mo(V) species still remains to be detected and/or identified as such among the various Mo(V) species observed so far. Additional kinetic, thermodynamic and spectroscopic investigations on Mo(V) species in soluble nitrate reductases are then required to progress on the understanding of their catalytic mechanism.

Supplementary data to this article can be found online at http://dx.doi.org/10.1016/j.bbabio.2013.10.013.

Acknowledgements

We would like to acknowledge the Aix-Marseille EPR spectroscopy Facility Center (national TGE-RENARD network, FR3443). This work was funded by the CNRS, CEA, Aix-Marseille Université and the Agence Nationale de la Recherche (ANR MC2 n°11-BSV5-005-01).

References

[1] P.J. Gonzalez, C. Correia, I. Moura, C.D. Brondino, J.J. Moura, Bacterial nitrate reductases: molecular and biological aspects of nitrate reduction, J. Inorg. Biochem. 100 (2006) 1015–1023.
[2] B. Bennett, B.C. Berks, S.J. Ferguson, A.J. Thomson, D.J. Richardson, Mo(V) electron paramagnetic resonance signals from the periplasmic nitrate reductase of Thiosphaera pantotropha, Eur. J. Biochem. 226 (1994) 789–798.
[3] S. Bursakov, M.Y. Liu, W.J. Payne, J. Legall, I. Moura, J.J.G. Moura, Isolation and preliminary characterization of a soluble nitrate reductase from the sulfate-reducing organism Desulfovibrio desulfuricans ATCC 27774, Anaerobe 1 (1995) 55–60.
[4] M. Sabaty, C. Avazeri, D. Pignol, A. Vermeglio, Characterization of the reduction of selenate and tellurite by nitrate reductases, Appl. Environ. Microbiol. 67 (2001) 5122–5126.
[5] T. Hettmann, R.A. Siddiqui, C. Frey, T. Santos-Silva, M.J. Romao, S. Diekmann, Mutagenesis study on amino acids around the molybdenum centre of the periplasmic nitrate reductase from Ralstonia eutropha, Biochem. Biophys. Res. Commun. 320 (2004) 1211–1219.
[6] B.J. Jepson, S. Mohan, T.A. Clarke, A.J. Gates, J.A. Cole, C.S. Butler, J.N. Butt, A.M. Hemmings, D.J. Richardson, Spectropotentiometric and structural analysis of the periplasmic nitrate reductase from Escherichia coli, J. Biol. Chem. 282 (2007) 6425–6437.
[7] P.J.L. Simpson, A.A. McKinzie, R. Codd, Resolution of two native monomeric 90 kDa nitrate reductase active proteins from Shewanella gelidimarina and the sequence of two napA genes, Biochem. Biophys. Res. Commun. 398 (2010) 13–18.
[8] R. Gangeswaran, D.J. Lowe, R.R. Eady, Purification and characterization of the assimilatory nitrate reductase of Azotobacter vinelandii, Biochem. J. 289 (1993) 335–342.
[9] B.J.N. Jepson, L.J. Anderson, L.M. Rubio, C.J. Taylor, C.S. Butler, E. Flores, A. Herrero, J.N. Butt, D.J. Richardson, Tuning a nitrate reductase for function - the first spectropotentiometric characterization of a bacterial assimilatory nitrate reductase reveals novel redox properties, J. Biol. Chem. 279 (2004) 32212–32218.
[10] T.H. Wang, Y.H. Chen, J.Y. Huang, K.C. Liu, S.C. Ke, H.A. Chu, Enzyme kinetics, inhibitors, mutagenesis and electron paramagnetic resonance analysis of dual-affinity nitrate reductase in unicellular N-2-fixing cyanobacterium Cyanothece sp PCC 8801, Plant Physiol. Biochem. 49 (2011) 1369–1376.
[11] P. Arnoux, M. Sabaty, J. Alric, B. Frangioni, B. Guigliarelli, J.M. Adriano, D. Pignol, Structural and redox plasticity in the heterodimeric periplasmic nitrate reductase, Nat. Struct. Biol. 10 (2003) 928–934.
[12] J.M. Dias, M.E. Than, A. Humm, R. Huber, G.P. Bourenkov, H.D. Bartunik, S. Bursakov, J. Calvete, J. Caldeira, C. Carneiro, J.J. Moura, I. Moura, M.J. Romao, Crystal structure of

the first dissimilatory nitrate reductase at 1.9 A solved by MAD methods, Structure 7 (1999) 65–79.
[13] S. Najmudin, P.J. Gonzalez, J. Trincao, C. Coelho, A. Mukhopadhyay, N.M. Cerqueira, C.C. Romao, I. Moura, J.J. Moura, C.D. Brondino, M.J. Romao, Periplasmic nitrate reductase revisited: a sulfur atom completes the sixth coordination of the catalytic molybdenum, J. Biol. Inorg. Chem. 13 (2008) 737–753.
[14] C. Coelho, P.J. Gonzalez, J.G. Moura, I. Moura, J. Trincao, M. Joao Romao, The crystal structure of Cupriavidus necator nitrate reductase in oxidized and partially reduced states, J. Mol. Biol. 408 (2011) 932–948.
[15] S. Metz, W. Thiel, Theoretical studies on the reactivity of molybdenum enzymes, Coord. Chem. Rev. 255 (2011) 1085–1103.
[16] S. Grimaldi, B. Schoepp-Cothenet, P. Ceccaldi, B. Guigliarelli, A. Magalon, The prokaryotic Mo/W-bisPGD enzymes family: a catalytic workhorse in bioenergetic, Biochim. Biophys. Acta 8–9 (2013) 1048–1085.
[17] N.M. Cerqueira, P.J. Gonzalez, C.D. Brondino, M.J. Romao, C.C. Romao, I. Moura, J.J. Moura, The effect of the sixth sulfur ligand in the catalytic mechanism of periplasmic nitrate reductase, J. Comput. Chem. 30 (2009) 2466–2484.
[18] H. Xie, Z. Cao, Enzymatic reduction of nitrate to nitrite: insight from density functional calculations, Organometallics 29 (2009) 436–441.
[19] M. Hofmann, Density functional theory study of model complexes for the revised nitrate reductase active site in Desulfovibrio desulfuricans NapA, J. Biol. Inorg. Chem. 14 (2009) 1023–1035.
[20] C.S. Butler, J.M. Charnock, B. Bennett, H.J. Sears, A.J. Reilly, S.J. Ferguson, C.D. Garner, D.J. Lowe, A.J. Thomson, B.C. Berks, D.J. Richardson, Models for molybdenum coordination during the catalytic cycle of periplasmic nitrate reductase from Paracoccus denitrificans derived from EPR and EXAFS spectroscopy, Biochemistry 38 (1999) 9000–9012.
[21] C.S. Butler, S.A. Fairhurst, S.J. Ferguson, A.J. Thomson, B.C. Berks, D.J. Richardson, D.J. Lowe, Mo(V) coordination in the periplasmic nitrate reductase from Paracoccus pantotrophus probed by electron nuclear double resonance (ENDOR) spectroscopy, Biochem. J. 363 (2002) 817–823.
[22] P.J. Gonzalez, M.G. Rivas, C.D. Brondino, S.A. Bursakov, I. Moura, J.J. Moura, EPR and redox properties of periplasmic nitrate reductase from Desulfovibrio desulfuricans ATCC 27774, J. Biol. Inorg. Chem. 11 (2006) 609–616.
[23] C.S. Butler, J.M. Charnock, C.D. Garner, A.J. Thomson, S.J. Ferguson, B.C. Berks, D.J. Richardson, Thiocyanate binding to the molybdenum centre of the periplasmic nitrate reductase from Paracoccus pantotrophus, Biochem. J. 352 (2000) 859–864.
[24] F. Biaso, B. Burlat, B. Guigliarelli, DFT investigation of the molybdenum cofactor in periplasmic nitrate reductases: structure of the Mo(V) EPR-active species, Inorg. Chem. 51 (2012) 3409–3419.
[25] V. Fourmond, B. Burlat, S. Dementin, P. Arnoux, M. Sabaty, S. Boiry, B. Guigliarelli, P. Bertrand, D. Pignol, C. Léger, Major Mo(V) EPR signature of Rhodobacter sphaeroides periplasmic nitrate reductase arising from a dead-end species that activates upon reduction. Relation to other molybdoenzymes from the DMSO reductase family, J. Phys. Chem. B 112 (2008) 15478–15486.
[26] V. Fourmond, M. Sabaty, P. Arnoux, P. Bertrand, D. Pignol, C. Léger, Reassessing the strategies for trapping catalytic intermediates during nitrate reductase turnover, J. Phys. Chem. B 114 (2010) 3341–3347.
[27] V. Fourmond, B. Burlat, S. Dementin, M. Sabaty, P. Arnoux, E. Etienne, B. Guigliarelli, P. Bertrand, D. Pignol, C. Léger, Dependence of catalytic activity on driving force in solution assays and protein film voltammetry: insights from the comparison of nitrate reductase mutants, Biochemistry 49 (2010) 2424–2432.
[28] S. Stoll, A. Schweiger, EasySpin, a comprehensive software package for spectral simulation and analysis in EPR, J. Magn. Reson. 178 (2006) 42–55.
[29] C.J. Kay, M.J. Barber, Measurement of oxidation-reduction midpoint potentials by room temperature electron paramagnetic resonance potentiometry, Anal. Biochem. 184 (1990) 11–15.
[30] A.G. Porras, G. Palmer, The room temperature potentiometry of xanthine oxidase. pH-dependent redox behavior of the flavin, molybdenum, and iron-sulfur centers, J. Biol. Chem. 257 (1982) 11617–11626.
[31] G.R. Hanson, I. Lane, Dimethylsulfoxide (DMSO) reductase, a member of the DMSO reductase family of molybdenum enzymes, in: G. Hanson, L. Berliner (Eds.), Metals in Biology Applications of High-Resolution EPR to Metalloenzymes, Springer, 2010, pp. 169–193.
[32] P. Bertrand, B. Frangioni, S. Dementin, M. Sabaty, P. Arnoux, B. Guigliarelli, D. Pignol, C. Léger, Effects of slow substrate binding and release in redox enzymes: theory and application to periplasmic nitrate reductase, J. Phys. Chem. B 111 (2007) 10300–10311.
[33] V. Fourmond, T. Lautier, C. Baffert, F. Leroux, P.-P. Liebgott, S. Dementin, M. Rousset, P. Arnoux, D. Pignol, I. Meynial-Salles, P. Soucaille, P. Bertrand, C. Léger, Correcting for electrocatalyst desorption and inactivation in chronoamperometry experiments, Anal. Chem. 81 (2009) 2962–2968.
[34] P. Bertrand, C. More, B. Guigliarelli, A. Fournel, B. Bennett, B. Howes, Biological polynuclear clusters coupled by magnetic interactions. From the point dipole approximation to a local spin model, J. Am. Chem. Soc. 116 (1994) 3078–3086.
[35] J. Caldeira, V. Belle, M. Asso, B. Guigliarelli, I. Moura, J.J.G. Moura, P. Bertrand, Analysis of the electron paramagnetic resonance properties of the [2Fe-2S]1 + centers in molybdenum enzymes of the xanthine oxidase family: assignment of signals I and II, Biochemistry 39 (2000) 2700–2707.
[36] D.J. Lowe, R.C. Bray, Magnetic coupling of molybdenum and iron-sulfur centers in xanthine oxidase and xanthine deshydrogenases, Biochem. J. 169 (1978) 471–479.
[37] C. More, M. Asso, G. Roger, B. Guigliarelli, J. Caldeira, J. Moura, P. Bertrand, Study of the spin-spin interactions between the metal centers of Desulfovibrio gigas aldehyde oxidoreductase: identification of the reducible sites of the [2Fe-2S]1 +,2 + clusters, Biochemistry 44 (2005) 11628–11635.
[38] S.J. Field, N.P. Thornton, L.J. Anderson, A.J. Gates, A. Reilly, B.J.N. Jepson, D.J. Richardson, S.J. George, M.R. Cheesman, J.N. Butt, Reductive activation of nitrate reductases, Dalton Trans. (2005) 3580–3586.
[39] V.L. Davidson, What controls the rates of interprotein electron-transfer reactions, Acc. Chem. Res. 33 (2000) 87–93.
[40] V.L. Davidson, Protein control of true, gated, and coupled electron transfer reactions, Acc. Chem. Res. 41 (2008) 730–738.
[41] R.A. Rothery, B. Stein, M. Solomonson, M.L. Kirk, J.H. Weiner, Pyranopterin conformation defines the function of molybdenum and tungsten enzymes, Proc. Natl. Acad. Sci. U. S. A. 109 (2012) 14773–14778.
[42] M.G. Bertero, R.A. Rothery, M. Palak, C. Hou, D. Lim, F. Blasco, J.H. Weiner, N.C.J. Strynadka, Insights into the respiratory electron transfer pathway from the structure of nitrate reductase A, Nat. Struct. Biol. 10 (2003) 681–687.
[43] D.P. Kloer, C. Hagel, J. Heider, G.E. Schulz, Crystal structure of ethylbenzene dehydrogenase from Aromatoleum aromaticum, Structure 14 (2006) 1377–1388.
[44] B. Bradshaw, D. Collison, C.D. Garner, J.A. Joule, Stable pyrano[2,3-]quinoxalines and pyrano[2,3-]pteridines related to molybdopterin, Chem. Commun. (2001) 123–124.
[45] P. Basu, S.J.N. Burgmayer, Pterin chemistry and its relationship to the molybdenum cofactor, Coord. Chem. Rev. 255 (2011) 1016–1038.
[46] J.H. Enemark, C.D. Garner, The coordination chemistry and function of the molybdenum centres of the oxomolybdoenzymes, J. Biol. Inorg. Chem. 2 (1997) 817–822.
[47] B.R. Williams, Y. Fu, G.P. Yap, S.J. Burgmayer, Structure and reversible pyran formation in molybdenum pyranopterin dithiolene models of the molybdenum cofactor, J. Am. Chem. Soc. 134 (2012) 19584–19587.
[48] B. Bradshaw, D. Collison, C.D. Garner, J.A. Joule, Synthesis of 1,3-dithiol-2-ones as proligands related to molybdopterin, Org. Biomol. Chem. 1 (2003) 129–133.
[49] S.J. Burgmayer, D.L. Pearsall, S.M. Blaney, E.M. Moore, C. Sauk-Schubert, Redox reactions of the pyranopterin system of the molybdenum cofactor, J. Biol. Inorg. Chem. 9 (2004) 59–66.
[50] S. Dementin, P. Arnoux, B. Frangioni, S. Grosse, C. Léger, B. Burlat, B. Guigliarelli, M. Sabaty, D. Pignol, Access to the active site of periplasmic nitrate reductase: insights from site-directed mutagenesis and zinc inhibition studies, Biochemistry 46 (2007) 9713–9721.
[51] S. Gardlik, K.V. Rajagopalan, Oxidation of molybdopterin in sulfite oxidase by ferricyanide. Effect on electron transfer activities, J. Biol. Chem. 266 (1991) 4889–4895.
[52] M.E. Helton, M.L. Kirk, A model for ferricyanide-inhibited sulfite oxidase, Inorg. Chem. 38 (1999) 4384–4385.